Thermal Hysteresis Phenomena in Micellar Solutions of Gangliosides: Theory and Experiments

Laura Cantu', Mario Corti, Elena del Favero, Elena Digirolamo, Antonio
Raudino

Thermal Hysteresis Phenomena in Micellar Solutions of Gangliosides: Theory and Experiments

Laura Cantu' (^{1}), Mario Corti (^{2}), Elena del Favero (^{1}), Elena Digirolamo (^{1}) and Antonio Raudino (^{3,*})

(^{1}) Study Center for Functional Biochemistry of Brain Lipids, Department of Medical Chemistry and Biochemistry, the Medical School, University of Milan, via Saldini 50, 20133 Milan, Italy
(^{2}) INFM-Department of Electronics, University of Pavia, via Abbiategrasso 209, 27100 Pavia, Italy
(^{3}) Department of Chemistry, University of Catania, viale A. Doria 6, 9515 Catania, Italy

Abstract. — Light scattering experiments show that micellar solutions of various gangliosides have a thermotropic behaviour which is irreversible with respect to temperature. Gangliosides, amphiphilic molecules of biological origin, form micelles in solution which decrease their average aggregation number upon heating. When a critical temperature is reached, any further cooling and heating cycle does not alter the micellar size. This process, not determined by a denaturation of the ganglioside molecule, is explained by considering the temperature-dependent coupling between micellar aggregation number and molecular conformation of ganglioside polar head groups. A simple model is proposed which assumes that the polar heads may exist in two different stable conformations, each of them with an energy dependent on its own internal structure and on the interactions with the surrounding heads at the micelle surface. The interconversion between the conformational minima is then described as a cooperative event, with a naturally emerging barrier due to collective effects which accounts for the experimentally observed irreversibilities. The model has some resemblances with the solidification process from an undercooled fluid, with the main difference that it deals with a *confined* two-dimensional system at the micellar surface.

1. Introduction

Gangliosides are amphiphilic molecules of biological relevance characterized by the presence of sugar moieties with different degree of complexity. They are abundant in neuronal plasma membranes [1] and are believed to be involved in processes like protein binding, cell recognition [2] and signal transduction [3]. Gangliosides have a marked amphiphilic character since they are double tailed amphiphilic molecules in which a ceramide portion, constituted mainly by C18 and C20 sphingosine and C18 fatty acid, carries a rather bulky headgroup made of several sugar rings, some of which can be sialic acid residues (Fig. 1). Differently from phospholipids, gangliosides can form globular aggregates like micelles or bilayer type structures
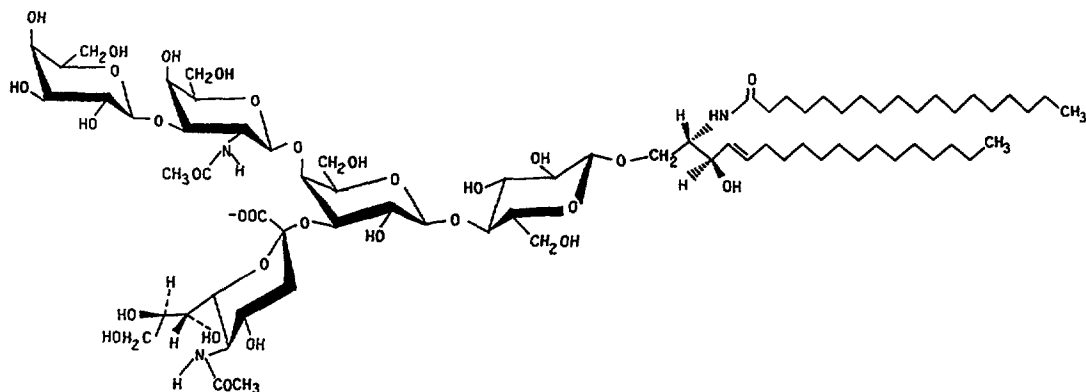

(*) Author for correspondence

Fig. 1. — Chemical structure of the ganglioside GM1.

like vesicles, according mainly to the complexity of the oligosaccharide chain headgroup. The aggregative properties of gangliosides have been extensively studied in water solution in the temperature range 25 °C – 30 °C as pure gangliosides or mixed with other natural or synthetic amphiphiles [4].

The present paper reports on the existence of a thermotropic behaviour of ganglioside micellar solutions which is irreversible with respect to temperature and is not due to denaturation of the molecules. This interesting thermodynamic process, carefully studied experimentally for the ganglioside GM1, is interpreted by means of a model which assumes the existence of two stable states in the landscape of possible conformations of ganglioside molecule in the aggregate. The interconversion between the two states, which involves a change in the conformational features of the hydrophilic portion of the molecule, is described as a cooperative event, with a naturally emerging barrier due to collective effects. The model has some resemblances with the solidification process from an undercooled fluid, with the important difference that applies to a confined two-dimensional system constrained by the micellar surface.

The conformational change in the ganglioside GM1 is observed experimentally through its aggregative properties. In fact, the globular arrangement of the micellar aggregate, which minimizes the unfavourable contact of water with the hydrophobic part of the molecules by creating an extended hydrophobic domain shielded by the layer of polar headgroups, is directly connected to the geometrical properties of the individual molecules. The geometrical properties are normally summarized in a dimensionless packing parameter [5], defined in terms of the area $\langle A \rangle$ occupied by the molecule at the hydrophobic-hydrophilic interface, the volume v and maximum extension l of the hydrophobic part of the molecule as $P = v/\langle A \rangle l$. The packing parameter assumes the limiting values $1/3$ for a cone and 1 for a cylinder. The corresponding aggregated structures are spheres and bilayers. Spherical micelles are obtained for $P < 1/3$ while non spherical micelles are obtained for $1/3 < P < 1/2$. In between these values, higher P's identify micelles with a more pronounced elliptical shape and larger aggregation number, and the closer is P to $1/2$, the larger are the variations of micellar dimension induced by geometrical changes in the molecules. The micellar aggregational state of gangliosides, which have packing parameter in the higher part of the micellar range close to $1/2$ (GM1 packing parameter varies from 0.428 to 0.411, depending on temperature), is therefore highly sensitive to reveal even a slight change in the ganglioside molecule conformation which modifies its geometrical hyndrance with no need of local probing, as the micellar aggregation number or,

equivalently, the micellar molecular mass is going to change. In particular, GM1 micelles have been observed by neutron and light scattering [4] to be globular and nicely represented by oblate ellipsoids with an axial ratio of the order of 2 and a hydrodynamic radius of 58 Å.

2. Experimental Results

The change of micellar average molecular weight is monitored in dilute solutions of the ganglioside GM1 by measuring the light intensity scattered at an angle of 90°. The scattered intensity is in fact proportional to the weight average mass of the micelles in solution, or equivalently to their average aggregation number N, since the molecular weight of the individual ganglioside molecule is fixed (1561 Dalton for GM1). Due to the small dimension of GM1 micelles, the scattered intensity does not have a significative dependence both on the scattering angle and on micellar shape [6].

The laser light scattering technique and the experimental apparatus are described elsewhere [6]. All samples are prepared at a concentration of 0.0015 g/cm³ by weighting the dry gangliosides and adding 30 mM NaCl solution at room temperature. NaCl keeps the ionic strength high enough to shield the electrostatic interactions among micelles [7].

Figure 2 shows the behaviour of the micellar aggregation number with temperature (^{1}). Point A is the value at room temperature. Micellar solutions prepared at room temperature below 30 °C are extremely stable, giving the same value of scattered intensity, corresponding to point A, even at one-year-time difference. Upon heating the solution, the micellar average aggregation number decreases considerably up to a temperature of 55 °C, path a. Then it stays practically constant at its lowest value, path b of Figure 2, either by further heating the solution or by cooling it down to room temperature (point B). At this stage, the micellar average aggregation number follows path b for any subsequent heating and cooling procedure. The micellar hydrodynamic radius, as measured by dynamic light scattering [6], varies consistently with the molecular weight along the cycle, that is, decreases during the temperature scan between 30 °C and 55 °C from 58 Å to 52 Å and then stays constant. Two extreme conditions can therefore be identified at room temperature: the "cold" and "warm" one. The "cold" solution, which has not been subjected to an heating cycle, and the "warm" one, which has been subjected to any heating cycle, are characterized by a different average micellar mass and a different behaviour on heating. Once the "warm" state is reached above 55 °C, the micellar average aggregation number keeps invariate for ever. In fact, scattered intensity measurements corresponding to different temperature scans performed on the same "warm" GM1 solution at different times, even with a delay of many months, show no detectable difference.

Thin Layer Chromatography analysis on the "warm" GM1 did not show the formation of any glycolipid derivatives, indicating that the observed behaviour is not due to any denaturation process. Furthermore, if a "warm" solution is dried and the solute redissolved in water, the new solution behaves exactly as a "cold" solution, that is, it undergoes the heating and cooling cycle of Figure 2, path a and then path b.

Irreversible cycles are obtained also for intermediate temperature changes between the extreme values of 30 °C and 55 °C. After the temperature is raised from 30 °C to an intermediate value, say 40 °C, the new value of micellar average aggregation number is smaller than the

---

(^{1}) The values of the micellar average aggregation number have been calculated by using for the refractive index increment the value $dn/dc = 0.147$ cm³/g, as measured for unheated GM1 solutions at $T = 25°$C. Slight variations of this value as a function of temperature or for heated GM1 solutions have not been measured and then not considered. This assumption does not alter the experimental picture, since the micellar hydrodynamic radius measurements, which do not depend on this parameter, are perfectly consistent with the reported values of aggregation number.
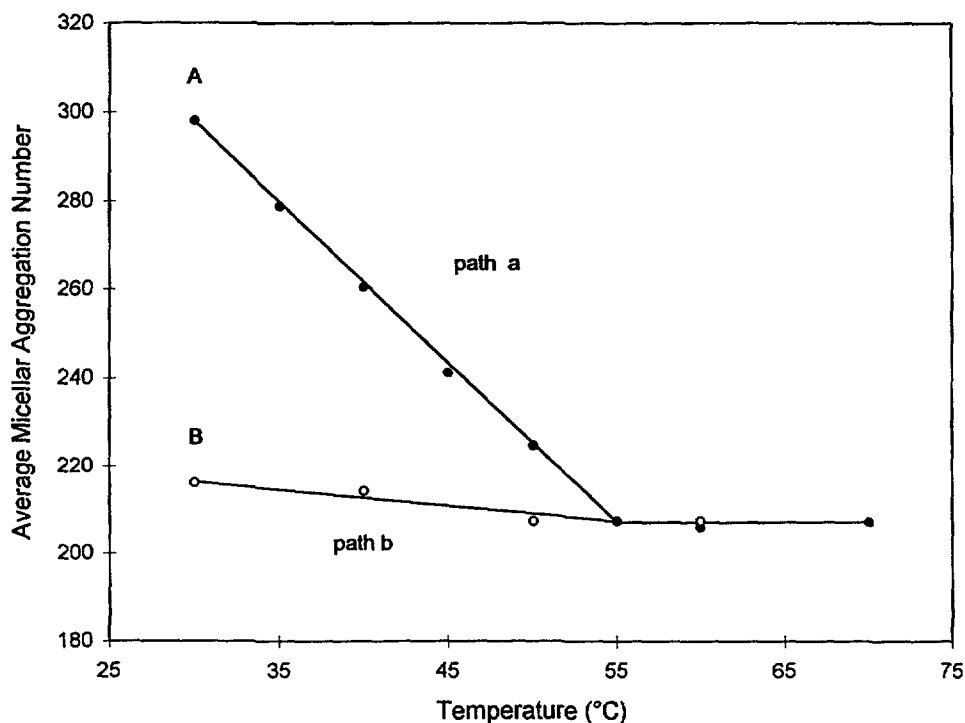
Fig. 2. — Variation of the micellar aggregation number during the temperature cycle as described in the text.

corresponding value at 30 °C and keeps practically unchanged for any subsequent cycle along which the temperature does not exceed 40 °C. Then, if the temperature is raised to a new value above 40 °C, say 50 °C, the average micellar aggregation number is lowered again to a value which remains practically constant as far as the system is kept below 50 °C. This happens until the system reaches the limiting "critical" temperature of 55 °C, above which micelles do not show to change their averaged aggregation number any more. Below the "critical" temperature the modification in the system depends on its thermal history. This is shown graphically in Figure 3, where the average aggregation number, measured at 25 °C, is reported as a function of the maximum temperature T_f reached in each heating-cooling cycle.

The scattered intensity values along the temperature cycles of Figure 2 have been taken at thermodynamic equilibrium by letting the system to equilibrate after each temperature step. In fact, after a temperature step along path a, the scattered intensity exponentially decays to the new value with an equilibration time which depends on the extent of the temperature step. The data of Figure 2 have been taken for steps of 5 °C, for which the equilibration time constant is of about 4 hours, this time being of the order of magnitude of ganglioside micellar lifetimes due to monomer exchange [8]. For larger temperature steps the equilibration times are shorter. Figure 4 shows measurements of the average micellar aggregation number performed as a function of temperature at a fast scan rate (0.5 °C per minute). The full lines are equilibrium path of Figure 2. Differences are quite significative along the heating cycle only.
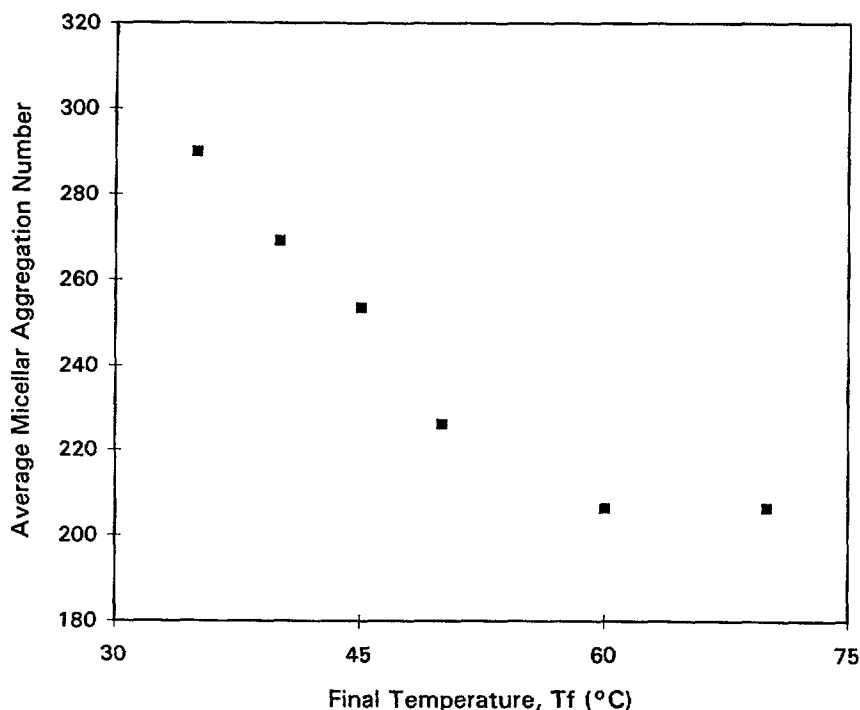
Fig. 3. — Average micellar aggregation number, measured at 25 °C, reported as a function of the maximum temperature T_f reached in each heating-cooling cycle, as described in the text.

3. Theoretical Modeling

Aim of this section is to propose some simplified models to investigate the temperature-dependent coupling between micellar aggregation number and molecular conformation of amphiphiles' polar head groups. Both equilibrium and metastable states will be considered in order to find possible explanations of thermal hysteresis phenomena experimentally observed.

For an isolated micelle of a given shape, the calculation of the aggregation number is reduced to the numerical estimate of amphiphile's surface area. Although the calculations can be performed for any micelle geometry, they turn out to be particularly simple in the case of spherical shape. Therefore, in order to retain a mathematical compactness and an easy understanding of the basic physic, we first consider spherical micelles, whereas a more general formalism developed for elliptical aggregates is contained in the Appendix C.

If, for simplicity, the micelle is assumed to be a sphere of radius R, made up of N monomers with average surface area $\langle A \rangle$ and constant molecular volume v, the obvious relationships: $Nv = \frac{4}{3}\pi R^3$ and $N\langle A \rangle = 4\pi R^2$ allows to express the aggregation number as a function of mean area

$$N = 36\pi \frac{v^2}{\langle A \rangle^3} \qquad (1)$$

Let us extend the above picture by assuming that the hydrophilic heads may exist in two different stable molecular conformations, each of them with an energy dependent on its own internal structure and on the interactions with the surrounding heads at the micelle surface. As far as gangliosides are concerned, detailed calculations on the isolated molecule evidenced the
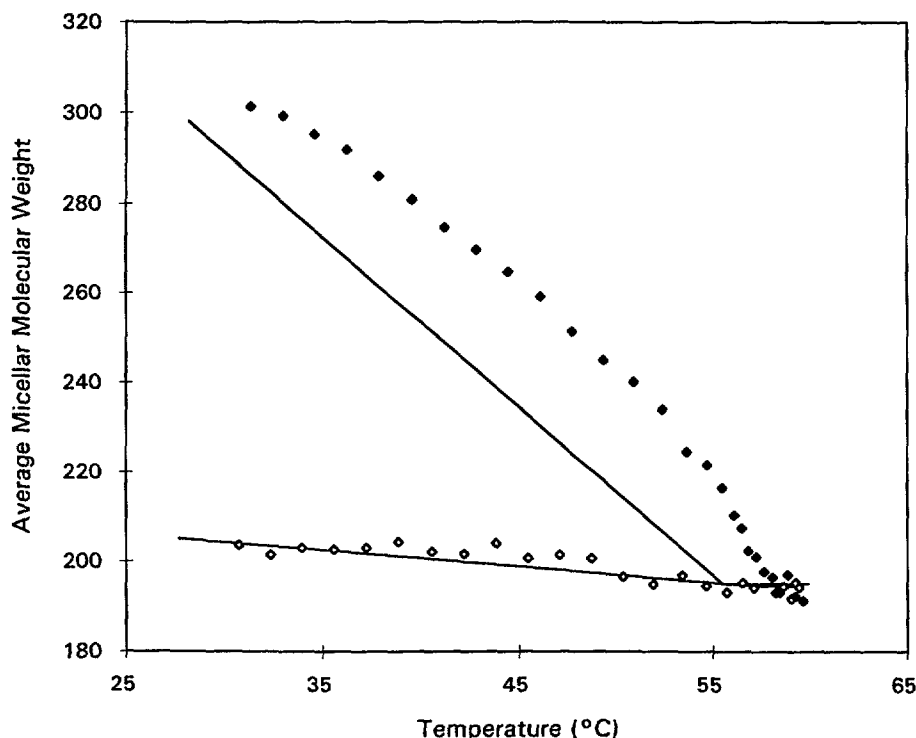
Fig. 4. — Measurements of the average micellar aggregation number performed as a function of temperature at a fast scan rate, 0.5 °C per minute. Full lines represent the equilibrium paths of Figure 2.

presence of two main conformations which are local minima in the free energy landscape [9], a result supported also by NMR measurements [10]. Interconversion among the minima could be very slow because of energy barriers. Once again, the barrier can be an intrinsic property of the ganglioside related to its own molecular structure or could depend on the collective interactions among the heads. Whether the barrier height is large, one expects the onset of non-equilibrium effects such the ones reported in the experimental section.

In order to draw a model which describes the interconversion between conformational minima one has to assume whether it is an "independent" or "cooperative" event. The fingerprints of the two different behaviours are not easy to recognize in the experimental observations. Anyway, the picture of micelle surface as a collection of independent hydrophilic heads existing in different internal states is rather unrealistic and leads to qualitative conclusions which are in contrast with the experimental findings.

For the sake of comparison, let us first briefly discuss the model of independent heads, the more complex picture of a cooperative transition model being addressed in the next subsections.

3.1. INDEPENDENT HEADS MODEL. — Let us consider a hydrophilic head with two internal states, the energy of which being E_1 and E_2, separated by a barrier of height E^* (see Fig. 5). We impose that at time $t = 0$ most of the heads lie, say, in 1. If E^* is small (compared to $k_B T$) and $E^* + |E_2|$ is large, we expect on heating from T_i to T_f a rapid transition from 1 to 2, hence the final distribution approaches the equilibrium one given by Boltzmann distribution. By cooling
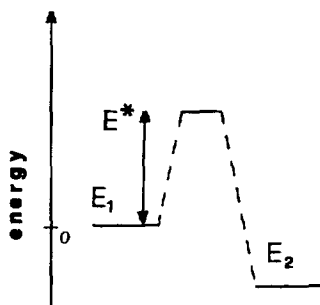
Fig. 5. — Energy diagram for the independent heads model. E_1, E_2 and E^* are the energies of two stable molecular conformations and that of the transition state, respectively.

from T_f to T_i the system might be unable to cross the high barrier with energy $E^* + |E_2|$, the heads remaining trapped in a metastable state the properties of which may differ from the equilibrium one. Furthermore, if the two conformations have different projected area onto micellar surface, according to equation (1) we must have a temperature-dependent variation of micelle aggregation number N, as well as the onset of thermal hysteresis on submitting the sample to heating and cooling cycles.

Albeit this simple model explains some experimental facts, it does not reproduce some interesting effects as described in Section 4. These shortcomings are removed in a model of cooperative transition which we are going to develop.

3.2. COOPERATIVE HEADS MODEL. — In this model we do not assume any intrinsic energy barrier among the conformations of hydrophilic heads, the barrier will be naturally emerging as a collective effect in a cooperative transition. The inclusion of an intrinsic barrier amongst the internal states of the heads does not change the physical picture, but probably some parameters have to be re-scaled.

3.2.1. Definition of Main Energy Contributions. — Assuming that the hydrophilic heads in a micellar aggregate may lie in two different conformational states (the population of which being η and $1 - \eta$, respectively) and letting A be the local surface area of the hydrophilic head, the total free energy can be written as: $F_{\text{tot}} = F_0 + \frac{1}{\langle A \rangle} \int_S F(A, \eta) dS$, where F_0 contains all the contributions to the free energy which do not depend on the local values of η and A as discussed in Appendix B, $\langle A \rangle$ is the mean surface area and the integration extended over the whole micelle surface. The implicit assumption contained in the above equation is that the hydrocarbon chain energy remains constant under rearrangements at water interface. An approximate but reliable expression for $F(A, \eta)$ is

$$F(A, \eta) = \gamma A + \frac{C(\eta)}{A} - TS(\eta) + H(\eta) \tag{2}$$

where γA is the interface energy (γ is the water-micelle interface tension), and the term $C(\eta)/A$ measures the strength of repulsion forces among the heads (electrostatic and excluded-volume interactions), consistent with a two-dimensional gas picture of amphiphiles surface. $TS(\eta)$ is the entropy contribution consequent to the mixing of heads belonging to two different states and finally the enthalpic contribution $H(\eta)$ is a measure of the internal energy difference among the conformations of amphiphile's head. Choosing units where the Boltzmann's constant is 1, the simplest expressions for mixing entropy and enthalpy are: $S(\eta) = -\eta \log \eta - (1-\eta) \log(1-\eta)$ and

$H(\eta) = \eta E_1 + (1-\eta)E_2$, where E_1 and E_2 are the internal energies of the two conformers. The coupling between η and A is contained in the term $C(\eta)/A$. By assuming that the parameter $C(\eta)$ can be written as $C(\eta) = C_0 + C_2\eta(1-\eta)$, where $C_0 > 0$ is a repulsive term independent of the conformational structure of the heads, while C_2 (either positive or negative) is a modulation of the repulsion forces related to preferential interactions among nearest neighbors belonging to like or dislike conformations. Positive values of C_2 mean stabilization of micelle regions where one conformation is prevailing, whereas negative values lead to a random distribution of both conformers.

For the sake of mathematical simplicity, we discuss separately the cases where the energy difference between the two conformers is small or large. In particular, we will focus in the following on the case of small energy differences, while the opposite situation will be discussed in Section 4.5.

In the limit of small $(E_1 - E_2)/T$, we must have $\eta \simeq 1/2$. Therefore, it is convenient to introduce a new variable ε defined as $\eta = (1 - \varepsilon)/2$ and expand the energy in power series of ε. By using polar coordinates, retaining terms up to ε^4 and rearranging one gets:

$$F_{\text{tot}} = F_0 + \frac{1}{\langle A \rangle} \int_S F(A,\varepsilon)\mathrm{d}S = F_0 + \frac{2\pi}{\langle A \rangle} \int_0^\pi \left[\frac{1}{2}\kappa_\varepsilon(\nabla\varepsilon)^2 + \frac{1}{2}\kappa_A(\nabla A)^2 + \gamma A + \frac{C_0^{\text{eff}}}{A} \right.$$
$$\left. - \frac{1}{2}(T_c(A) - T)\varepsilon^2 + \frac{1}{4}b\varepsilon^4 + h\varepsilon \right] R^2 \sin\vartheta \mathrm{d}\vartheta \qquad (3)$$

where

$$C_0^{\text{eff}} \equiv C_0 + \frac{1}{4}C_2$$
$$T_c(A) \equiv \frac{1}{2}\frac{C_2}{A}$$
$$b \equiv T/3$$
$$h \equiv \frac{1}{2}(E_2 - E_1)$$
$$(\nabla\varepsilon)^2 \equiv \frac{1}{R^2}\left(\frac{\partial\varepsilon}{\partial\vartheta}\right)^2 \;,\; (\nabla A)^2 \equiv \frac{1}{R^2}\left(\frac{\partial A}{\partial\vartheta}\right)^2$$

the integration being performed over the whole surface of a sphere of radius R. The two terms: $(1/2)\kappa_\varepsilon(\nabla\varepsilon)^2 + (1/2)\kappa_A(\nabla A)^2$ take into account the strength of the system against spatial inhomogeneities both of conformational composition and surface area.

Equation (3) is of Landau-Ginzburg type for the "order parameter" ε under the effect of a "field" h; the parameter ε is non conservative because there are no relationships among the populations of the two conformers. In the limit $\varepsilon \Rightarrow 0$ and A independent of position over micelle surface, the energy functional (3) is identical to that introduced by Israelachvili, Ninham and Mitchell [5] to calculate the surface area A of amphiphile aggregates. In the present model composition (ε) and geometrical (A) variables are coupled through the term $T_c(A) \cdot \varepsilon^2$ which gives rise to several effects as it will be discussed shortly.

The equilibrium values for the conformational composition and surface area can be determined by free energy minimization with respect to ε and A. Moreover, lateral phase separation, leading to the formation of domains richer in molecules belonging to a particular conformation, can be easily calculated in the framework of a mean-field model.

Non-equilibrium values can be assumed by ε and A giving rise to hysteretic behaviour which can be accounted for by investigating the time evolution of area (A) and composition (ε). A simple approach is as follows.
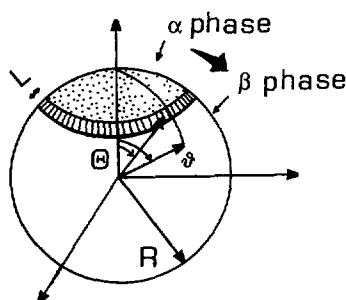
Fig. 6. — Geometrical parameters used to describe the growing of the α-phase against the β-phase on the surface of a spherical micelle. The hatched zone of thickness L and angular position Θ is the transition region between the two phases.

3.2.2. Phase Transition Kinetics.

— The time evolution of a generic "order parameter" can be described by a time-dependent Landau-Ginzburg equation. Assuming as variational parameters the composition ε and the surface area A, we write:

$$\Gamma_\varepsilon \frac{\partial \varepsilon}{\partial t} = -\frac{\delta F_{\text{tot}}}{\delta \varepsilon} \tag{4a}$$

$$\Gamma_A \frac{\partial A}{\partial t} = -\frac{\delta F_{\text{tot}}}{\delta A} \tag{4b}$$

where Γ_ε and Γ_A are friction coefficients for the evolution of ε and A, F_{tot} is the free energy of the system defined by equation (3) and the symbols $\delta F_{\text{tot}}/\delta \varepsilon$ and $\delta F_{\text{tot}}/\delta A$ mean the functional derivatives of the free energy with respect to ε and A: $\delta F_{\text{tot}}/\delta \varepsilon = \partial F_{\text{tot}}/\partial \varepsilon - \nabla \partial F_{\text{tot}}/\partial(\nabla \varepsilon)$ (analogous expression holds for $\delta F_{\text{tot}}/\delta A$). Namely, the functional derivatives describe the thermodynamic force driving the system toward equilibrium.

As we shall see shortly, the functional described by equation (3) has, in general, two stable solutions both for the variable ε and A (these roots are labeled as ε_+, A_+ and ε_-, A_-). Another (ε, A) pair represents a maximum in the free energy and will not be considered. This means that, for certain values of temperature or other relevant physical parameters, two phases (referred to as α and β) characterized by a particular conformational population and surface area, coexist.

Therefore, in the present model, hysteresis effects are related to the rate of appearance of a phase (and disappearance of the parent phase), rates that, generally, differ from each other to a large extent.

In order to calculate the rate of phase propagation, we assume that a particular solution of the system of equations (4) is compatible with the motion of a well defined interface which propagates without distortion (a "soliton") as described in Figure 6. This is due to the quartic terms in the free energy functional which lead to cubic non-linearities in the time-dependent Landau-Ginzburg equations (4) characterized by soliton-like solutions.

From a mathematical standpoint, we look for a solution of the form:

$$\varepsilon = \varepsilon(\theta - \Theta(t)) \quad ; \quad A = A(\theta - \Theta(t)) \tag{5}$$

Equation (5) describes an interfacial profile which is preserving its initial shape during front propagation (see Fig. 6 for the definition of the symbols). By defining $u \equiv \theta - \Theta(t)$, using the relationships

$$\frac{\partial \varepsilon}{\partial t} = -\dot{\Theta}\frac{\partial \varepsilon}{\partial u}, \quad \frac{\partial A}{\partial t} = -\dot{\Theta}\frac{\partial A}{\partial u} \tag{6}$$

($\dot{\Theta} = d\Theta(t)/dt$), combining equations (4) and (6) and integrating over the whole micelle surface, we find after simple algebra

$$\dot{\Theta} = \frac{1}{\Gamma_\varepsilon I_\varepsilon + \Gamma_A I_A} \int_S \left[\frac{\delta F}{\delta \varepsilon} \frac{\partial \varepsilon}{\partial u} + \frac{\delta F}{\delta A} \frac{\partial A}{\partial u} \right] dS \tag{7}$$

$I_\varepsilon \equiv \int_S (\partial \varepsilon / \partial u)^2 \, dS$, $I_A \equiv \int_S (\partial A / \partial u)^2 \, dS$. By setting $\dot{\Theta} = 0$, that is for identical rates for the growing of the α and β phases, the critical angle Θ_c, which corresponds to the "critical extension" of coexisting α and β phases on the same micelle, can be calculated from equation (7) by solving the equation

$$\int_S \left[\frac{\delta F}{\delta \varepsilon} \frac{\partial \varepsilon}{\partial u} + \frac{\delta F}{\delta A} \frac{\partial A}{\partial u} \right] dS = -\frac{\partial}{\partial \Theta} \int_S F(\varepsilon, A) dS = 0 \tag{8}$$

The free energy F calculated at $\Theta = \Theta_c$ allows to determine the barrier for the transition from α to β (and *vice versa*), which is going to be estimated in the following.

In order to solve equation (8) we have to know the profile of ε and A at the micelle surface. Exact analytical calculation starting from equations (3) and (8) is feasible for planar geometries and, likely, even in spherical coordinates with some additional complexities. Much simpler results can be obtained by the following reasoning. Indeed, as previously discussed, both ε and A are practically constant before of the propagation front (Fig. 6), their values being ε_-, A_- (α phase). Then, a sudden transition region, of the order of a few molecular diameters, separates α and β. Finally, a new phase, β, defined by constant ε_+ and A_+ values is reached. A good interpolation formula is

$$\varepsilon = G(\varepsilon_\pm, \theta) \tag{9a}$$

with $G \equiv G(\varepsilon_\pm, \theta)$ defined as:

$$\begin{aligned} G &= \varepsilon_- & 0 \le \theta \le \Theta - \Theta_0 \\ G &= \frac{1}{2}(\varepsilon_+ + \varepsilon_-) + \frac{1}{2}(\varepsilon_+ - \varepsilon_-)) \frac{\theta - \Theta_0}{\Theta_0} & \Theta - \Theta_0 \le \theta \le \Theta + \Theta_0 \\ G &= \varepsilon_+ & \Theta + \Theta_0 \le \theta \le \pi \end{aligned} \tag{9b}$$

where $\Theta_0 \propto L/R \ll 1$ is the (angular) width of the discontinuity between α and β phases (see Fig. 6), with L of the order of $A^{1/2}$. An analogous expression can be written for the profile of A

$$A = G(A_\pm, \theta) \tag{10}$$

where $G(A_\pm, \theta)$ has the same analytical form of $G(\varepsilon_\pm, \theta)$, equations (9), with $\varepsilon_\pm$ replaced by $A_\pm$.

In order to employ the above equations (9) and (10), we need an estimate of the pairs $\varepsilon_\pm$, $A_\pm$ (the composition and area inside α and β homogeneous phases). As already said, this calculation is easily performed by minimizing F_{tot} (Eq. (3)) with respect to ε and A. By neglecting gradient terms like $(\nabla \varepsilon)^2$ and $(\nabla A)^2$ because they vanish inside spatially homogeneous phases, straightforward calculations give

$$\frac{\partial F_{\text{tot}}}{\partial \varepsilon} = -(T_c(A) - T)\varepsilon + b\varepsilon^3 + h = 0 \tag{11a}$$

$$\frac{\partial F_{\text{tot}}}{\partial A} = \gamma - \frac{C_0^{\text{eff}}}{A^2} - \frac{\partial T_c(A)}{\partial A} \varepsilon^2 = 0 \tag{11b}$$

Equation (11a) has three distinct roots, but we consider only those defining energy minima, denoted by ε_+ and ε_-.

Even equation (11b), coupled to (11a) through the term $\varepsilon^2 \partial T_c(A)/\partial A$, has multiple roots, the roots corresponding to energy minima being A_+ and A_-. By treating h as a perturbation (the opposite case for large h will be considered in Sect. 4.5), and recalling that $C_2/C_0^{\text{eff}} \ll 1$, we look for a perturbation solution of equations (11): $\varepsilon_\pm = \varepsilon_\pm^{(0)} + \varepsilon_\pm^{(1)} + \varepsilon_\pm^{(2)} +$ \qquad A little algebra gives

$$\varepsilon_\pm^{(0)} = \pm((T_c(A_\pm^{(0)}) - T)/b)^{1/2} \tag{12a}$$

higher order terms are

$$\varepsilon_\pm^{(1)} = -\frac{h^{(1)}}{2gb\varepsilon_\pm^{(0)^2}} \simeq -\frac{h^{(1)}}{2b\varepsilon_\pm^{(0)^2}} \tag{12b}$$

$$\varepsilon_\pm^{(2)} = -\frac{h^{(1)^2}}{8g^2b^2\varepsilon_\pm^{(0)^5}}\left(1 - \frac{C_2^3}{16\gamma^2 gbA_\pm^{(0)^5}}\right) \simeq -\frac{h^{(1)^2}}{8b^2\varepsilon_\pm^{(0)^5}} \tag{12c}$$

with $g \equiv 1 - C_2^2/8\gamma bA_\pm^{(0)^3} \simeq 1$.

Analogously: $A_\pm = A_\pm^{(0)} + A_\pm^{(1)} + A_\pm^{(2)} + \ .$ \quad A simple calculation shows that $A_\pm^{(0)}$ satisfies the cubic equation $A^{(0)^3} + a_1 A^{(0)} + a_0 = 0$ ($a_1 \equiv -(C_0^{\text{eff}} + C_2 T/2b)/\gamma$, $a_0 \equiv C_2^2/4\gamma b$). Solution of the cubic equation, followed by a perturbation calculation, eventually yields a compact expression for $A_\pm^{(i)}$

$$A_\pm^{(0)} = (C_0^{\text{eff}}/\gamma)^{1/2}\left[1 + \frac{T}{4b}\frac{C_2}{C_0^{\text{eff}}} + \mathbf{O}((C_2/C_0^{\text{eff}})^2)\right] \tag{13a}$$

$$A_\pm^{(1)} = \frac{h^{(1)}}{4gbA_\pm^{(0)}\varepsilon_\pm^{(0)}} \simeq \frac{h^{(1)}}{4bA_\pm^{(0)}\varepsilon_\pm^{(0)}} \tag{13b}$$

$$A_\pm^{(2)} = \frac{C_2 h^{(1)^2}}{8g^2b^2 A_\pm^{(0)}\varepsilon_\pm^{(0)^4}}\left(1 - \frac{C_2}{4\gamma A_\pm^{(0)^2}} - \frac{3C_2^3}{32gb\gamma^2 A_\pm^{(0)^5}}\right)$$

$$\simeq \frac{C_2 h^{(1)^2}}{8b^2 A_\pm^{(0)}\varepsilon_\pm^{(0)^4}} \tag{13c}$$

From equations (12, 13) the useful relationships $\varepsilon_-^{(0)} = -\varepsilon_+^{(0)}, \varepsilon_-^{(1)} = \varepsilon_+^{(1)}, \varepsilon_-^{(2)} = -\varepsilon_+^{(2)}$ are found. Analogously: $A_-^{(0)} = A_+^{(0)}, A_-^{(1)} = -A_+^{(1)}, A_-^{(2)} = A_+^{(2)}$.

By combining the above equations (see the Appendix A for details), it can be proved that minimization procedure reported by equation (8) yields

$$\frac{\partial}{\partial \Theta}\int_S F(\varepsilon, A)\mathrm{d}S = \frac{\partial}{\partial \Theta}(E_0 + A\cos\Theta + B\sin\Theta) = 0 \tag{14}$$

where

$$E_0 \equiv F_0 + \gamma A^{(0)} + \frac{C_0^{\text{eff}}}{A^{(0)}} - \frac{1}{4}b\varepsilon^{(0)^4}$$

$$A \equiv \left(\frac{2}{15}b\varepsilon^{(0)^2} + \frac{\kappa_\varepsilon}{2R^2\Theta_0^2}\right)\Theta_0\varepsilon^{(0)^2}$$

$$B \equiv \frac{9}{8}\varepsilon^{(0)}h^{(1)}$$

As already said, the solution of equation (14) gives the value of the "critical angle", which then obeys the following

$$\text{tg } \Theta_c = \frac{A}{B} \tag{15}$$

and the total free energy at $\Theta = \Theta_c$ can be obtained from equation (3) and it is the maximum value of F_{tot}

$$F_{\text{tot}}^{\max} = N(E_0 + (A^2 + B^2)^{1/2}) \tag{16}$$

The transition probability from α (characterized by the ε_-, A_- pair) to the β phase (characterized by ε_+, A_+ pair) (or *vice versa*) is proportional, in the Transition State approximation, to $\exp((F_{\text{tot}}(\varepsilon_\pm, A_\pm) - F_{\text{tot}}^{\max})/T)$. After replacing $F_{\text{tot}}(\varepsilon_\pm, A_\pm)$ and $F_{\text{tot}}^{\max}$ by their analytical expressions and a little rearrangement, the transition probabilities (rates) can be obtained

$$v_+ = k(T) \exp(+\mu(T)Nh^{(1)}/T) \tag{17a}$$

$$v_- = k(T) \exp(-\mu(T)Nh^{(1)}/T) \tag{17b}$$

where $v_\pm$ are the rates for the α to β phase transition (or *vice versa*). $k(T)$ is the mean rate. It depends on several parameters, but (this is a key point) is identical for both forward (from α to β) and backward (from β to α) transition, hence its analytical expression is unessential for our purposes. The function $\mu(T)$ is defined as

$$\mu(T) \equiv \frac{3^{5/2}}{2^3} \left[\frac{T_c(A^{(0)}) - T}{T} \right]^{1/2} \geq 0 \tag{18}$$

Then, even if $h^{(1)}/T$ is small (as assumed at the beginning of our calculations), the product $Nh^{(1)}/T$ (N being the micelle aggregation number) can be very large, and consequently the forward and backward rates can be strongly different.

3.2.3. Temperature Variation of Micelle Aggregation Number. — In the previous section it was shown how the rate of transition between two phases, which are dissimilar for conformational structure and area, is an activated process. Moreover, $\alpha \Rightarrow \beta$ and $\beta \Rightarrow \alpha$ transition rates differ to a large extent (see Eqs. (17a,b)), according to the relative stability of the conformers. It is easy to see that conformational population (ε) and amphiphile surface area (A) are coupled (see Eqs. (12, 13)), so that conformational changes may induce strong variations in the surface area. In turn, according to equation (1), surface area increase implies a decrease of micelle aggregation number N.

For the sake of comparison with experimental data, which are averaged properties over a macroscopic sample containing a large number of micelles, the next step requires the calculation of the temperature-dependent mean area, which is experimentally observed as a temperature-dependent average aggregation number, of a collection of non-interacting micelles.

Two different kinds of calculation will be performed.

The first assumes an equilibrium (Boltzmann) distribution, namely temperature-dependent changes are allowed for the area and composition within each phase and as well for the number of micelles lying in α and β phases. This picture is valid when both the interconversion kinetics $\alpha \Rightarrow \beta$ and $\beta \Rightarrow \alpha$ are reasonably fast.

A second picture holds when the two rates differ to a large extent and non-equilibrium effects are likely. In fact, under the assumption that one of the interconversion rates is very slow, only the area and composition within each phase are allowed to be temperature-dependent parameters, while the ratio α-micelles/β-micelles is practically constant.

In an equilibrium description the probabilities for a micelle to exist in α or β state $P_+(T)$, $P_-(T)$ depend on the actual temperature and the mean area $\bar{A}$ of a collection of micelles is

$$\bar{A} = P_+(T)A_+(T) + P_-(T)A_-(T) \tag{19}$$

(where $A_\pm(T) \simeq \langle A_\pm(T)\rangle$, the bracketts denoting homogeneous phase, namely we assume that micelles lie either in α or β phase, only a few of them belonging to transient states as those depicted in Figure 6 where both α and β phases coexist). The normalized probability $P_\pm(T)$ for a micelle to belong to α or β can be calculated as reported in Appendix B, the resulting expressions, satisfying the normalization condition $P_+(T) + P_-(T) = 1$, are

$$P_+(T) \quad = \quad \frac{\exp(-\Delta F_{\text{tot}}/T)}{1 + \exp(-\Delta F_{\text{tot}}/T)}(1 + G) \tag{20a}$$

$$P_-(T) \quad = \quad \frac{1}{1 + \exp(-\Delta F_{\text{tot}}/T)}(1 - G\exp(-\Delta F_{\text{tot}}/T)) \tag{20b}$$

where $\Delta F_{\text{tot}} \equiv F_{\text{tot}}(\varepsilon_+, A_+) - F_{\text{tot}}(\varepsilon_-, A_-)$ and the analytical expression of G is reported in Appendix B. The correction term G arises from the different translational entropy of α and β micelles which have different aggregation numbers.

Combining equations (19, 20) with the expression for the free energy $F_{\text{tot}}(\varepsilon, A)$ (Eq. (3)) and retaining terms up to the second order, after a little algebra the following equation can be obtained

$$\bar{A}_{\text{eq}} \cong A^{(0)}(T) + A^{(2)}(T) - \frac{1}{T}A^{(1)}(T)F_{\text{tot}}(\varepsilon^{(1)}(T), A^{(1)}(T)) + \frac{A^{(1)^2}(T)}{A^{(0)}(T)}\rho \tag{21}$$

with $\rho \equiv 3(1 + \log(\mathbb{C}/2))$, $\mathbb{C}$ being the total micelles concentration, and $\varepsilon^{(k)}$ and $A^{(k)}$ defined by equations (12, 13). A noticeable simplification of equation (21) is achieved by exploiting symmetry relationships among the functions $\varepsilon_\pm^{(k)}$ and $A_\pm^{(k)}$ reported past equations (13). This allows to express the mean area $\overline{A}_{\text{eq}}$ as a function of $A^{(k)} \equiv A_+^{(k)}$ and $\varepsilon^{(k)} \equiv \varepsilon_+^{(k)}$ alone.

Let us investigate the non-equilibrium variation of the mean area with temperature. In this case the increase of micelle area depends on thermal history of the sample. For the sake of simplicity, let us assume the interconversion rates $v_\pm$ ($\alpha \Rightarrow \beta$ and $\beta \Rightarrow \alpha$, defined by Eq. (17)) to be infinite and zero, respectively. Moreover, we impose that at time $= 0$ all micelles are, say, in the α phase. After heating, the number of micelles belonging to α and β classes tends to equate. Next, we cool the sample. Some micelles remain trapped within a metastable state and the number of micelles in α and β is determined by the maximum heating temperature T_f rather than by the actual temperature T : $P_+(T) \cong P_+(T_f)$. By imposing this constraint to equation (21), the non-equilibrium mean area is

$$\bar{A}_{\text{N-eq}} \cong A^{(0)}(T) + A^{(2)}(T) - \frac{1}{T_f}A^{(1)}(T)F_{\text{tot}}(\varepsilon^{(1)}(T_f), A^{(1)}(T_f)) + \frac{A^{(1)}(T_f)A^{(1)}(T)}{A^{(0)}(T)}\rho \tag{22}$$

($\overline{A}_{\text{N-eq}}$ = non-equilibrium mean area). By comparing equations (21, 22) and relating $\overline{A}$ to the mean aggregation number $\overline{N}$ by equation (1), one finds after straightforward algebra [11]

$$\bar{N}_{\text{N-eq}}(T) \simeq \bar{N}_{\text{eq}}(T)(1 + |\lambda|\zeta(T, T_f)) \tag{23}$$

where

$$|\lambda| \quad \equiv \quad \frac{81}{16}\frac{T_c(A^{(0)})}{\gamma A^{(0)}}h^{(1)^2} \tag{24a}$$

$$\zeta(T, T_f) \quad \equiv \quad \frac{1}{T^{1/2}T_f^{3/2}}\left[\frac{T_c(A^{(0)}) - T_f}{T_c(A^{(0)}) - T}\right]^{1/2} - \frac{1}{T^2} \tag{24b}$$

Since $\zeta(T, T_f) \leq 0$, $T_c(A^{(0)}) > T_f$ and $T < T_f$, we find the non-equilibrium variation of the aggregation number $\overline{N}$ with temperature be weaker than at equilibrium. Furthermore, it depends on thermal history of the sample through T_f (the maximum heating temperature). Some numerical data will be discussed in the next section and compared with available experimental data.

4. Discussion of Theoretical and Experimental Results

At a first sight, the model developed so far has some resemblances with the process of solidification from an undercooled fluid, the main self-evident difference being in the coupling between amphiphiles' conformational states and surface area which determines variations of micelle aggregation number. A deeper analysis reveals interesting effects related to the confined geometry of micellar suspensions. Two further differences are:

A) The phase transition (see Fig. 6) takes place onto the surface of a *lone* micelle. Hence, a dilute micellar suspension can be depicted as a collection of independent bodies, each of them statistically undergoing a phase transition. The resulting situation is very different from undercooled homogeneous fluids where once the growing phase has reached a critical size, the transition proceeds until the new phase pervades all the sample and, therefore, sharper variations with temperature are generally found.

B) Within a continuous homogeneous fluid the critical size of the growing phase may take any value, as determined by the forces involved in the transition process. By contrast, within a micelle the critical size of the growing phase cannot exceed micelle radius (Fig. 6). This fact imposes severe constraints to the activation energy, as shown by equations (14) to (18).

Besides these general aspects highlighting the peculiar behavior of systems with confined (and curved) geometry, the model predicts a number of effects which are discussed as follows.

4.1. GENERAL CONDITIONS TO HAVE HYSTERESIS PHENOMENA. — The cooperative model developed so far clearly shows how the temperature-dependent aggregation number is different when operating at equilibrium or non-equilibrium conditions. This happens when the following conditions are fulfilled:

a) there are at least two internal conformational states of the heads of amphiphiles. These states must be local minima in the energy landscape, but there are no restrictions on the height of the barrier among the minima (by contrast, the independent heads model poses severe constraints to the height of the interconversion barriers, see Sect. 3.1).

b) The interactions among heads with identical molecular conformation must be energetically stronger than those among heads with opposite conformation. This is the key factor of the cooperative model. (The independent heads model is, of course, independent of intermolecular interactions strength).

c) The heat bath temperature must be smaller than the difference between like-like and like-dislike interactions (i.e. $T_c(A) > T$, see Eq. (3)), otherwise thermal hysteresis disappears. At variance of the cooperative model, the independent heads picture does not predict vanishing of non-equilibrium phenomena with temperature, rather it suggests a slow approaching of forward and backward rates, reducing the width of thermal hysteresis.

The hysteresis phenomenon on the micellar average aggregation number is clearly observed experimentally for the ganglioside GM1 as shown in Figure 2. Path a refers to the equilibrium temperature-dependent average aggregation number, while path b is the non-equilibrium one.
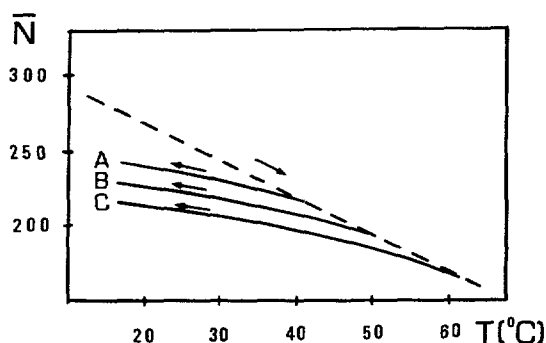
Fig. 7. — Non-equilibrium mean aggregation number $\bar{N}_{N-eq}$ *vs.* temperature for cooling process. The discontinuous line is the hypothetical equilibrium curve assumed to be a straight line ($\bar{N}_{eq} = 1000 - 2.5\,T$). The values have been calculated from equation (23) by using the following parameters: $T_c = 400$ K, $|\lambda| = 5 \times 10^4$ deg^2, $T_f = 40$ °C (curve A), 50 °C (curve B) and 60 °C (curve C).

The experimental data validate the collective model since hysteresis effects sharply disappear above 55 °C, which can be considered as the "critical" temperature T_c of Section 3.2.

4.2. "INTERMEDIATE" HYSTERESES. — The collective model predicts a kind of thermal behavior which will be referred to as "intermediate" hysteresis. With the name of "intermediate" hystereses a topology like that reported in Figure 7 is defined, where after heating ($i_0 \Rightarrow f_j$, with $j = 1, 2, ...$) and cooling cycles (f $\Rightarrow i_0$) the aggregation numbers are arranged as $\bar{N}(f_1) \geq \bar{N}(f_2) \geq \bar{N}(f_3) \geq$; namely, in a thermal cycle (where initial and final temperatures are identical), micelle mean aggregation number is remaining different.

The curves in Figure 7 have been calculated from equation (23) using the parameters reported in the figure legend and by assuming a linear equilibrium heating curve (discontinuous curve). All hystereses are of "intermediate" type and are practically parallel to each other, their relative spacing being linearly related to the maximum heating temperature $T_f = T(f_j)$ ($j = 1, 2, $.). Furthermore, it can be easily seen from equation (23) that the slope of non-equilibrium aggregation number $\bar{N}_{N-eq}$ *vs.* T is always smaller than at equilibrium.

The "intermediate" hysteresis behavior is easily understood by the arguments developed in Section 3.2. Both composition (molecules in 1 or 2 conformation within α and β phases) and number of micelles lying in α and β change with temperature. After heating from an initial, say T_i, to final, say T_f, temperature, the sample is cooled again to T_i. Since a fast $\alpha \Rightarrow \beta$ interconversion rate but a vanishing backward rate has been assumed, some micelles remain trapped into metastable states during non-equilibrium cooling. Therefore, only temperature dependent conformational composition (and related surface area) within each phase is allowed, while the number of micelles trapped in a particular state remains practically constant.

The "intermediate" hysteresis effects, predicted by the cooperative model as sketched in Figure 7, are clearly observed experimentally. The non-equilibrium paths are rather flat and all parallel to path b of Figure 2, with decreasing average aggregation number for increasing values of the final temperature T_f (with $T_f < T_c$) reached in the cycle. For graphical clarity these intermediate hysteresis paths (which behave as curves A, B and C of Fig. 7) are not reported in Figure 2, but Figure 3 gives the micellar average aggregation number at the initial temperature $T_i = 25$ °C after a full intermediate cycle with maximum temperature T_f (namely $T_i \Rightarrow T_f \Rightarrow T_i$) as a function of T_f. In other words, Figure 3 reports the spacing among the "intermediate" hystereses as defined in Figure 7 (curves A, B and C). The behaviour is almost linear, as predicted by the collective model, with a break at the critical temperature T_c.

4.3. EFFECT OF THE HEATING RATE ON THERMAL HYSTERESIS. — Although the α to β transition has been assumed to be fast as compared with the reverse kinetics, it requires a finite time, its rate being defined by equation (17b). Therefore, when the heating rate is too fast, the number of micelles lying in α and β phases does not change. It is easy to prove that the non-equilibrium aggregation number $\overline{N}_{N-eq}$ depends upon T according to

$$\bar{N}_{N-eq}(T) = \tilde{N}_{eq}(T)(1 + |\lambda|\zeta(T, T_i)) \tag{25}$$

where T_i is the initial temperature of the sample and $\zeta(T, T_i) \geq 0$ is defined through equation (24b) with T_i instead of T_f. The proof of equation (25) is fully analogous to that used to derive equation (23) and is not repeated; one must keep in mind that equation (25) is valid only for fast heating modes, hence it is just the upper limit of the true value.

Equation (25) is able to reproduce the experimental data of Figure 4 in that the predicted $N_{N-eq}(T)$ is larger than $N_{eq}(T)$ for $T < T_c$. The increase in slope at high T can be explained by considering that the energy barrier to α to β transition is small. Then, the absence (or lowering) of non-equilibrium phenomena at high temperatures is conceivable because the height of the barrier is less fundamental in determining the process rate, hence one expects a variation of $\bar{N}$ vs. T typical for processes at equilibrium.

4.4. MONOMERS-MICELLE EXCHANGE DOES NOT AFFECT THERMAL HYSTERESIS. — Previous works unambiguously showed monomer exchange among ganglioside micelles [8] and ganglioside-phospholipid vesicles [12] a phenomenon common to all amphiphilic assemblies. Therefore, one could hypothesize that micelles lying in a particular conformation might evolve toward more stable structures through monomer exchange across the aqueous medium where monomers may, or may not, retain their own original molecular conformation.

This levelling mechanism is not allowed in our cooperative model. Indeed, one must keep in mind that α and β phases (each of them characterized by a well-defined conformational composition and surface area) are two energy minima, they are divided by an energy barrier, the height of which being roughly proportional to $((T_c - T)/T^2)$. Hence, any variation of conformational composition consequent to monomer uptake from water causes a rearrangement of the system either through monomers escape from micelle or by conformational rearrangement onto micelle surface in order to react to the displacement from equilibrium. This behavior, common both to micelles lying in stable (absolute energy minimum) and metastable (relative energy minimum) states, can explain how thermal hysteresis is persisting even in the presence of monomer exchange among micelles, as experimentally observed.

It is interesting to notice that this last prediction on the influence of monomer exchange on thermal hysteresis, which is a consequence of the collective model, would come out just the opposite through the independent heads picture developed in Section 3.1. In the "independent heads" situation, in order to maintain constant the conformational population within the micelle (a necessary condition to get hysteresis), one must impose that the monomer is preserving its own molecular conformation both at micelle surface and during its transfer across the aqueous medium, an assumption unvalid in most cases because of the different environments. Hence, the independent heads model is sensitive to monomer exchange which may reduce, or even abolish, the onset of non-equilibrium phenomena.

4.5. THERMAL HYSTERESIS DEPENDENCE ON CONFORMATIONAL ENERGY DIFFERENCE OF AMPHIPHILIC HEADS. — The cooperative transition theory has been developed in the limit of small h/T (h proportional to the energy difference between two amphiphile conformations, see Eq. (3)) and large $(T_c - T)/T$ (strong segregation limit). To stress the perturbation nature of the parameter h, we used the notation $h^{(1)}$ throughout. The theory shows that for small $h^{(1)}$
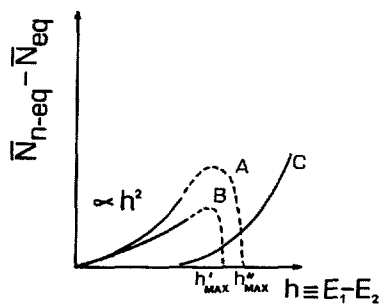
Fig. 8. — Schematic variation of the thermal hysteresis magnitude (defined as the difference between equilibrium and non-equilibrium aggregation number of the micelles) against the dimensionless h parameter, a measure of the energy difference between the two stable conformations of lipid heads. Curves A and B have been obtained for two different of critical temperature T_c ($T_c(A) > T_c(B)$). Curve C: independent heads model.

thermal hysteresis is proportional to $h^{(1)^2}$ (see Eqs. (23)-(25)), next we want to investigate what happens in the limit of large $h^{(1)}$. From the cubic equation (11a) (setting for the sake of simplicity $T_c(A) \simeq T_c$, independent of A) it is easy to see that the three real roots coalesce to a single real value (one-phase system) when h reaches $h_{\max}$ defined as

$$\frac{h_{\max}}{T} = \frac{2}{3}((T_c - T)/T)^{3/2} \qquad (26)$$

namely, when $h \geq h_{\max}$ all micelles lie in a single stable phase and there is no hysteresis.

A qualitative sketch of this behavior is given in Figure 5 where the mean non-equilibrium aggregation number $\bar{N}_{N-eq}$ (setting as a reference the equilibrium one) vs. h is reported. The plot clearly shows the existence of a narrow "window" of h values which may induce thermal hysteresis. Indeed, very small h means a biphasic systems where the two phases interchange from each other at the same rate, whereas large h determines only a stable one-phase system. The width of the "window" increases on raising the critical temperature T_c, namely strong interactions among heads with identical conformation favour thermal hysteresis. Furthermore, looking at equation (24a), one observes that non-equilibrium effects are enhanced by low micelle-water interfacial tension γ. Molecules like gangliosides bearing bulky hydrophilic sugar units could have lower interfacial tension than other small-sized head group amphiphiles.

Summarizing, the onset of thermal hysteresis in cooperative systems requires: i) strong interactions among heads with identical conformation (i.e. large T_c, greater than the heat bath temperature); ii) low interfacial tension (large and flexible hydrophilic heads); iii) conformational energy difference of amphiphiles' head restricted to a narrow range.

Completely different are the predictions of the independent heads model. Indeed, assuming a large difference between forward and backward interconversion rates, together with the condition of a fast forward rate ($|E^*|/T \ll 1$, according to Fig. 5), we conclude that hysteresis onset requires ($|E_1 - E_2|)/T \equiv 2|h|/T \gg 1$. Namely, huge amphiphile's conformational energy difference must be involved (see Fig. 8, curve C).

4.6. POLYDISPERSITY OF THE AGGREGATION NUMBER.

— Our theory predicts that the polydispersity of the aggregation number depends on thermal history of the sample. To be more specific, at a given temperature the distribution of the aggregation number about its

mean value $\bar{N}$ should be broader and more asymmetric in samples submitted to a thermal cycle (heating from T_i to T_f and cooling from T_f to T_i) than for untreated samples. Enhanced polydispersity after thermal cycles is related to metastable trapping of micelles in different configurations, each of them characterized by a particular aggregation number, as already discussed in the previous sections, and is not repeated here.

Nevertheless this polydispersity increase is not accessible experimentally in the real GM1 solution made of small-sized micelles with a slight but non negligible intrinsic polydispersity.

4.7. DEVIATION FROM THE SPHERICAL SHAPE. — Most micelles, like GM1 ganglioside investigated in this paper, deviate from the spherical shape. A more general theory accounting for ellipsoidal geometries has been developed and is briefly described in Appendix C. The main results are: a) The difference between the growth and dissolution rates for a phase nucleating at the surface of ellipsoidal micelles is slightly greater than that observed in spherical aggregates (Eqs. (C.8a,b)). b) At variance of the spherical case, in ellipsoidal micelles the variation of non-equilibrium average aggregation number *vs.* temperature contains an additional multiplicative term which depends on eccentricity alone (Eq. (C.10)). When stable (equilibrium) and metastable (non-equilibrium) micelles have identical deviations from the spherical shape this term goes to 1. Even for large differences of eccentricity this term turns out to be a trivial multiplicative constant which modifies the numerical values but leaves unaltered the general topology of thermal hysteresis phenomena as reported in Figure 7. Only if the micellar shape of the stable state undergoes stronger variations with temperature than in the metastable state (or *vice versa*), one should expect some alterations of thermal hysteresis curves. This case has been never observed in GM1 ganglioside micelles.

5. Concluding Remarks

The existence of a well-defined critical temperature at which hysteresis effects sharply disappear is a clear evidence of the validity of the collective model here presented. Therefore, cooperativity plays an important role in the interconversion between the two aggregational states of gangliosides. This fact can be biologically relevant since the immunoactivity of gangliosides, which are known to produce clusters on artificial and natural membranes [13, 14], is found only when their concentration in membranes is large [15].

The physical mechanism involved in the interconversion between the two conformational states of the ganglioside molecule is not definitely known yet, but it is probably connected to a different degree of hydration which causes a tilt angle between its hydrophobic and hydrophilic portions. Temperature could, in fact, changes the relative interplay of the hydrogen bonding of the water solvent molecules with the ganglioside and the inter- and intramolecular hydrogen bonding of the OH and NH groups with the glucosidic oxygen in the ganglioside molecule. This hypothesis is suggested by the fact that also other gangliosides like GM2 and GD1a, which differ from GM1 in the length of the saccharidic portion but keep unchanged hydrophobic-hydrophilic boundary region, have been observed to undergo similar irreversibility effects [16] with a critical temperature similar to that of GM1, about 55 °C. It is worth noting that GT1b ganglioside does not exhibit any thermal hysteresis [16]. This means that the energy difference between the two conformations is not the same for the various gangliosides, but strongly depends on the chemical structure of the saccharidic head.

Finally, it is important to point out that there is no doubt that the reported thermotropic behaviour of GM1, in the temperature range between 30 °C and 55 °C, is due to a conformational change which involves the oligosaccharide chain of the ganglioside molecule and not to a flexibility effect of its hydrophobic portion. In fact, the double-chain hydrophobic

portion of gangliosides is common to other amphiphiles (*e.g.* phospholipids) which do not exhibit appreciable hysteresis effects. Moreover, the melting transition of the hydrocarbon tails of GM1 occurs around a temperature which is out of the investigated range, as reported in the literature [17]. Anyway let us now make the hypothesis that the melting temperature is inside the investigated range. Then, going through the transition on heating the hydrocarbon chains should increase their flexibility giving rise to a larger packing parameter [18] and then an increase of aggregation number should be observed rather than a reduction. Besides, lowering the temperature, the chains should go through the same transition backwards. This does not happen, and in fact, the micelle is now different. One may again argue that the melting transition temperature has changed. But this has to be due to something else than the chains themselves, for example a different headgroup conformation which allows a different packing of the chains. So, any possible hypothesis falls back to the initial statement that a change in the headgroup conformation has to be involved in the process. Going back to the initial temperature of 30 °C after the temperature scan, one observes a reduction in the micellar aggregation number from which one can calculate [19] a variation in the packing parameter from $P = 0.428$ to $P = 0.411$. This corresponds to an increase in the average area occupied by the headgroup at micellar surface from 95 Å^2 to 99 Å^2.

Acknowledgments

Appendix A

Aim of this appendix is the solution of the equation

$$\frac{\partial}{\partial\Theta}\int_S F(\varepsilon, A)\mathrm{d}S = 0 \tag{A.1}$$

By combining equations (8)-(10) with equations (12, 13) and the free energy functional, equation (3), and after tedious but straightforward algebra, equation (A.1) can be written as

$$\frac{\partial}{\partial\Theta}\int_S F(\varepsilon, A)\mathrm{d}S = N\sum_{k=1}^3 f_k = 0 \tag{A.2}$$

where $N = 4\pi R^2/\langle A\rangle$ is the micelle aggregation number and the functions f_k are as follows

$$f_1 \equiv \int_0^{\Theta-\Theta_0} F(\varepsilon_-, A_-)\sin\theta\mathrm{d}\theta = [\gamma A^{(0)} + \frac{C_0^{\mathrm{eff}}}{A^{(0)}} - \frac{1}{4}b\varepsilon^{(0)4}$$
$$-\frac{9}{8}\varepsilon^{(0)}h^{(1)}](1 - \cos\Theta - \Theta_0\sin\Theta) + \mathrm{O}(\Theta_0^2, h^{(1)^2}) \tag{A.2a}$$

$$f_2 \equiv \int_{\Theta-\Theta_0}^{\Theta+\Theta_0} F(\varepsilon(\theta), A(\theta))\sin\theta\mathrm{d}\theta = [2(\gamma A^{(0)} + \frac{C_0^{\mathrm{eff}}}{A^{(0)}}$$
$$-\frac{7}{30}b\varepsilon^{(0)4} + \frac{\kappa_\varepsilon}{R^2\Theta_0^2}\varepsilon^{(0)2}]\Theta_0\sin\Theta + \mathrm{O}(\Theta_0^2, h^{(1)^2}) \tag{A.2b}$$

$$f_3 \equiv \int_{\Theta+\Theta_0}^\pi F(\varepsilon_+, A_+)\sin\theta\mathrm{d}\theta = [\gamma A^{(0)} + \frac{C_0^{\mathrm{eff}}}{A^{(0)}} - \frac{1}{4}b\varepsilon^{(0)4}$$
$$+\frac{9}{8}\varepsilon^{(0)}h^{(1)}](1 - \cos\Theta - \Theta_0\sin\Theta) + \mathrm{O}(\Theta_0^2, h^{(1)^2}) \tag{A.2c}$$

where, in deriving equations (A.2) the identities $\varepsilon_-^{(0)} = -\varepsilon_+^{(0)} \equiv -\varepsilon^{(0)}$ and $A_-^{(0)} = A_+^{(0)} \equiv A^{(0)}$ have been repeatedly used together with the following integrals $I_n \equiv \Theta_0^{-n} \int_{\Theta-\Theta_0}^{\Theta+\Theta_0} (\theta - \Theta)^n \sin\theta d\theta$, calculated from standard tables [20]

$$I_{2n} = \frac{2}{2n+1} \Theta_0 \sin\Theta + O(\Theta_0^3) \tag{A.3a}$$

$$I_{2n+1} = \frac{2}{2n+3} \Theta_0^2 \cos\Theta + O(\Theta_0^4) \tag{A.3b}$$

with the aid of the above relationships, we obtain equation (14) of the main text.

Appendix B

Following standard equilibrium thermodynamics arguments, the relative population among m species with aggregation numbers N_1, N_2, . N_i, . N_m arises from the balance of the corresponding chemical potentials:

$$\mu_{N_i}^{(0)} + \frac{T}{N_i} \log(X_i/N_i) = \mu_{N_j}^{(0)} + \frac{T}{N_j} \log(X_j/N_j) \tag{B.1}$$

where the logarithm terms describe the concentration-depending entropic contribution to the chemical potential, X_i and X_j being the concentrations (mole fraction) of i-th and j-th component, whereas $\mu_i^{(0)}$ and $\mu_j^{(0)}$ are the self free energy per amphiphile which can be calculated from equation (3) once the minimum energy values of A and ε are known.

The $m-1$ equations (B.1) together with the mass conservation constraint: $X_1 + X_2 + .. + X_m = X_{\text{tot}}$ allows one to calculate the different X_i. Let us apply the above equations to a system where the self energy of the aggregate has sharp minima at $N \cong N_+$ and $N \cong N_-$, assuming that the two classes of micelles are in equilibrium with monomers and imposing mass conservation, we get after simple algebra

$$\frac{X_-}{(X_{\text{tot}} - X_1 - X_-)^\nu} = \frac{N_-}{N_+^\nu} \exp\left[N_- \frac{\mu_+^{(0)} - \mu_-^{(0)}}{T} \right] \tag{B.2}$$

where $\nu \equiv N_-/N_+$. According to the classical theory of micellization, above certain amphiphiles' critical concentration (CMC) X_1 remains practically constant ($X_1 \cong$ CMC), independent of the total amount of amphiphile molecules [5], allowing us to solve equation (B.2) for X_-. When ν is close to 1, we may employ a power series expansion. Taking the logarithm of equation (B.2), expanding in power series of $\nu - 1$ and solving the resulting expression by a standard perturbation procedure we get after straightforward algebra

$$X_- \cong (X_{\text{tot}} - X_1) \frac{\exp(-\Delta F_{\text{tot}}/T)}{1 + \exp(-\Delta F_{\text{tot}}/T)} [1 + \frac{\nu-1}{1 + \exp(-\Delta F_{\text{tot}})} (1 + \log\frac{\mathbf{C}}{1 + \exp(-\Delta F_{\text{tot}})})] \tag{B.3}$$

where $\Delta F_{\text{tot}} \equiv F_{\text{tot}}(\varepsilon_+, A_+) - F_{\text{tot}}(\varepsilon_-, A_-)$ and $\mathbf{C}$ is the total micellar concentration. It is easy to see that

$$\nu - 1 = \frac{N_- - N_+}{N_+} = \frac{A_+^3 - A_-^3}{A_-^3} \cong 6\frac{A^{(1)}}{A^{(0)}} \tag{B.4}$$

where in deriving equation (B.4) the identities $A_+^{(0)} = A_-^{(0)} \equiv A^{(0)}$ and $A_-^{(1)} = -A_+^{(1)} \equiv -A^{(1)}$ together with equation (1) have been used. Therefore, letting $X_-/(X_{\text{tot}} - X_1)$ be the normalized

probability P_- to have a micelle with aggregation number N_-, eventually we get equation (20a) of the main text, where the function G is defined as

$$G \equiv 6 \frac{A^{(1)}/A^{(0)}}{1 + \exp(-\Delta F_{\text{tot}})} [1 + \log \frac{C}{1 + \exp(-\Delta F_{\text{tot}})}] \qquad (B.5)$$

which is a slowly varying function of total micelle concentration C. Analogously, by imposing mass conservation we can easily calculate the probability P_+ reported in equation (20b).

Appendix C

Aim of this appendix is to extend the theory to the case of ellipsoidal micelles.

Starting from the relationships $N\langle A\rangle = \int_S dS$ (where N is the averaged aggregation number and $\langle A\rangle$ the mean surface area of micelle forming amphiphile) and $Nv = \int_V dV$ (v being amphiphile molecular volume) and expressing the surface and volume integrals as a function of ellipse eccentricity e, the following equation is derived

$$N = 36\pi \frac{v^2}{\langle A\rangle^3}(1 + \sigma(e)) \qquad (C.1)$$

where $\sigma(e)$ depends on the eccentricity alone. Letting a and b be the ellipse's axes, elementary geometry yields $\sigma(e) = \frac{1}{8}[(1 - e^2)^{1/2} + \frac{\arcsin e}{e}]^3 \frac{1}{(1-e^2)^{1/2}} \cong \frac{2}{15}e^4 + \mathbf{O}(e^6)$, with $e^2 \equiv (a^2 - b^2)/a^2$ ($a > b$, oblate ellipsoid) and $\sigma(e) = \frac{1}{8}[(1 + e^2)^{1/2} + \frac{1}{e}\log(e + (1 + e^2)^{1/2})]^3 \frac{1}{(1-e^2)^{1/2}} \cong e^2 + \frac{19}{30}e^4 + \mathbf{O}(e^6)$, with $e^2 \equiv (b^2 - a^2)/b^2$ ($b > a$, oblate ellipsoid). Hence, apart from a multiplicative term which is depending on e alone, the relationship between aggregation number and surface is identical both for spherical and ellipsoidal micelles. When $e = 0$ we recover equation (1) of the main text.

Let us turn to the much more complex problem of phase growing at the surface of an ellipsoidal micelle. The geometry adopted by us is reported in Figure 9 where two different reference frames have been employed. The rotated frame $X'Y'Z'$ defines the principal axes of an oblate ellipsoid (short axis along X'). In an arbitrary point of the micelle surface the α-phase grows against the β-phase and the boundary between the two phases is set at $\theta = \Theta$. In the rigid frame the equation defining micelle surface can be calculated as follows. In the $X'Y'Z'$ coordinates system the ellipsoid equation reads: $(X'/a)^2 + (Y'/b)^2 + (Z'/b)^2 = 1$. Then, we rotate the reference frame around Y' by employing an unitary rotation matrix:

$$\begin{vmatrix} X' \\ Z' \\ Y' \end{vmatrix} = \begin{vmatrix} \cos\omega & \sin\omega & 0 \\ -\sin\omega & \cos\omega & 0 \\ 0 & 0 & 1 \end{vmatrix} \begin{vmatrix} X \\ Z \\ Y \end{vmatrix} \qquad (C.2)$$

Finally, transforming the Cartesian coordinates X, Y and Z into spherical polar coordinates $R(\theta, \phi)$, θ and ϕ (see Fig. 9) we get

$$R \equiv R(\theta, \phi) = \frac{b}{(1 + e^2 f(\theta, \phi))^{1/2}} \qquad (C.3)$$

where

$$f(\theta, \phi) \equiv \sin^2\theta \cos^2\phi \cos^2\omega + \cos^2\theta \sin^2\omega + 2\sin\theta \cos\theta \sin\omega \cos\omega \cos\phi.$$
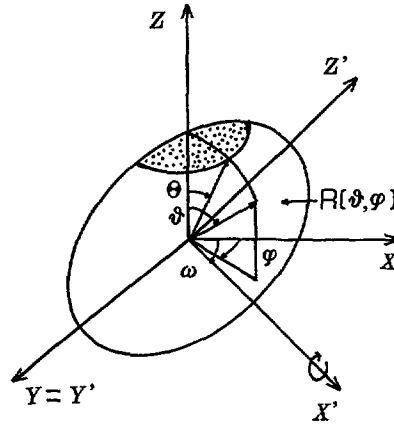
Fig. 9. — Geometrical parameters describing the growing α-phase (dotted region) on the surface of an oblate ellipsoidal micelle. The rotated frame $X'Y'Z'$ defines the ellipsoid axes, the rigid frame XYZ determines, through the angle Θ, the size of the phase α nucleating in an arbitrary point of micelle surface.

The free energy functional for a spherical micelle which may exist in different conformational states is described by equation (3) of the main text, the more general expression for an aggregate bounded by an arbitrary convex surface can be written as:

$$
\begin{aligned}
F_{\text{tot}} &= F_0 + \frac{1}{\langle A \rangle} \int_S F(A, \varepsilon) \mathrm{d}S \\
&= F_0 + \frac{1}{\langle A \rangle} \int_0^{2\pi} \mathrm{d}\phi \int_0^{\pi} \mathrm{d}\theta [\frac{1}{2}\kappa_\varepsilon (\nabla \varepsilon)^2 + \frac{1}{2}\kappa_A (\nabla A)^2 + \gamma A + \frac{C_0^{\text{eff}}}{A} \\
&\quad - \frac{1}{2}(T_c(A) - T)\varepsilon^2 + \frac{1}{4}b\varepsilon^4 + h\varepsilon]\sqrt{g(\theta, \phi)}
\end{aligned}
\tag{C.4}
$$

where [21]

$$
\sqrt{g(\theta, \phi)} = R^2 \sin\theta [1 + \frac{1}{R^2}(\partial R/\partial\theta)^2 + \frac{1}{R^2 \sin^2\theta}(\partial R/\partial\phi)^2]^{1/2}
\tag{C.4a}
$$

and

$$
\begin{aligned}
(\nabla\varepsilon)^2 &= \frac{1}{g(\theta, \phi)}[R^2 \sin^2\theta(\partial\varepsilon/\partial\theta)^2 + R^2(\partial\varepsilon/\partial\phi)^2 + ((\partial\varepsilon/\partial\theta)(\partial R/\partial\phi) \\
&\quad - (\partial\varepsilon/\partial\phi)(\partial R/\partial\theta))^2]
\end{aligned}
\tag{C.4b}
$$

(An analogous equation holds for $(\nabla A)^2$). As for the spherical case, we assumed a constant value of ε and A inside the α- and β-phases, joined by a linear interpolation law in the narrow boundary between the two phases (see Eqs. (9) and (10)). Simplification of equation (C.4b) is achieved noticing that $\partial\varepsilon/\partial\phi = \partial A/\partial\phi = 0$.

By exploiting the analytical expression for $R \equiv R(\theta, \phi)$ obtained in equation (C.3) we may calculate with the aid of equations (C.4a,b) the total free energy for an ellipsoidal micelle. Assuming that the growing phase can nucleate with identical probability at any point of micelle surface, the average total free energy turns out to be

$$
\langle F_{\text{tot}} \rangle_\omega = F_0 + \frac{1}{2\pi\langle A \rangle} \int_0^{2\pi} \int_S F(\varepsilon, A) \mathrm{d}S \, \mathrm{d}\omega
\tag{C.5}
$$

As discussed in the main text, the calculation of the critical size for a growing phase can be performed by solving equation (8) once the free energy functional F_{tot} is known. Hence, by combining equations (8) and (C.5) we get:

$$\frac{\partial}{\partial \Theta}\langle F_{\text{tot}}\rangle_\omega = \frac{\partial}{\partial \Theta}\int_0^{2\pi}\int_S F(\varepsilon, A)\mathrm{d}S\ \mathrm{d}\omega = 0 \qquad (C.6)$$

The evaluation of the integral (C.6) follows the same procedure developed in Appendix A. However, the eccentricity-dependent terms prevents one to obtain compact analytical expressions. If one limits the analysis to small eccentricities through an expansion in power series of e, the integration over the trigonometric functions is elementary. After tedious algebra one gets

$$\langle F_{\text{tot}}\rangle_\omega = \text{const.} + N[(A\sin\Theta + B\cos\Theta)(1 + \frac{1}{3}e^2) - \frac{1}{4}e^2\xi(\Theta)] + \mathbf{O}(e^4) \qquad (C.7)$$

where the A and B parameters (identical both for spherical and ellipsoidal micelles) have been defined by equation (14) and the function $\xi(\Theta)$ is

$$\xi(\Theta) \equiv \frac{4}{15}b\varepsilon^{(0)^4}\Theta_0(1 - \cos^2\Theta)\sin\Theta - \frac{9}{4}\varepsilon^{(0)}h^{(1)}(1 + \frac{1}{3}\cos^2\Theta)\cos\Theta \qquad (C.8)$$

Minimizing equation (C.7) with respect to Θ allows us to calculate the energy barrier to the $\alpha \Rightarrow \beta$ transition. Retaining the leading terms eventually we obtain a very compact expression for the forward ($\alpha \Rightarrow \beta$) and backward ($\beta \Rightarrow \alpha$) phase transition:

$$v_+ = K(T,e)\exp(+(1 + \frac{1}{3}e^2)\mu(T)Nh^{(1)}/T) + \mathbf{O}(e^4) \qquad (C.9a)$$

$$v_- = K(T,e)\exp(-(1 + \frac{1}{3}e^2)\mu(T)Nh^{(1)}/T) + \mathbf{O}(e^4) \qquad (C.9b)$$

where $K(T,e)$ is the mean component of the rate (identical for v_+ and v_-), the analytical expression of which is unessential, and the other symbols have been defined by equations (17, 18). By comparing this result with equation (18) of the main text it follows that the differences between forward and backward reactions rates are always greater in ellipsoidal than in spherical micelles.

The last task is the evaluation of the temperature-dependent averaged aggregation number for a collection of non-interacting micelles. This goal can be accomplished for calculating the micelle surface area as described in equations (19)-(22) of the main text and by relating the surface area to the averaged aggregation number through equation (1) (spherical micelles) or (C.1) (ellipsoidal micelles). Calculations have been performed both in equilibrium (stable) and non-equilibrium (metastable) states as thoroughly discussed in the theoretical Section 3.2.3. The final equation is rather similar to equation (23) obtained for the spherical case

$$\bar{N}_{\text{N-eq}}(T) \cong \bar{N}_{\text{eq}}(T)\frac{1 + \sigma(e_{\text{N-eq}})}{1 + \sigma(e_{\text{eq}})}(1 + |\lambda|\zeta(T, T_{\text{f}})) \qquad (C.10)$$

$\bar{N}_{\text{N-ex}}$ and $\bar{N}_{\text{eq}}$ being the averaged aggregation numbers in non-equilibrium and equilibrium conditions, respectively, and the functions $|\lambda|$ and $\zeta(T, T_{\text{f}})$ have been defined by equations (24a,b) of the main text. The function $\sigma(e)$ depends on non-spherical shape of micellar aggregate and is defined in equation (C.1) (analytical expressions for $\sigma(e)$ are exact, useful limits are: $\sigma(e) = 0$ for a sphere, $\sigma(e) \cong e^2 + \mathbf{O}(e^4)$ for an oblate ellipsoid and $\sigma(e) = \mathbf{O}(e^4)$ for a prolate ellipsoid). Since micelles may assume different eccentricities either in equilibrium (e_{eq})

or non-equilibrium states (e_{N-eq}), the shape-dependent term $1 + \sigma(e_{N-eq})/1 + \sigma(e_{eq})$ could differ from unity. The consequences of non-spherical shape on thermal hysteresis are discussed in Section 4.7.

References

[1] Tettamanti G., Sonnino S., Ghidoni R., Masserini M. and Venerando B., in Physics of Amphiphiles. Micelles, Vesicles and Microemulsions, V. Degiorgio and M. Corti Eds. (North-Holland, Amsterdam, 1985) pp. 607-636; Hakomori S.I., *Ann. Rev. Biochem.* **50** (1981) 733; Wiegandt H., *New Compr. Biochem.* **10** (1985) 199.

[2] Curatolo W., *Biochim. Biophys. Acta* **906** (1987) 137.

[3] Fishman P. J., *Membr. Biol.* **69** (1982) 85.

[4] Sonnino S., Cantu' L., Corti M., Acquotti D. and Venerando B., *Chem. Phys. Lipids* **71** (1994) 21; Corti M. and Cantu' L., in Non Medical Applications of Liposomes, Y. Barenholtz and D. Lasic Eds. (CRC Press, Boca Raton (FL) 1995) pp. 219-236.

[5] Israelachvili J.N., Mitchell D.J. and Ninham B.W., *J. Chem. Soc. Faraday Trans. 2* **72** (1976) 1525.

[6] Corti M., in Physics of Amphiphiles: Micelles, Vesicles and Microemulsions, V. Degiorgio and M. Corti Eds. (North Holland, Amsterdam, 1985) pp. 122-151.

[7] Cantu' L., Corti M. and Degiorgio V., *Faraday Discuss. Chem. Soc.* **83** (1987) 287.

[8] Cantu' L., Corti M. and Salina P., *J. Phys. Chem.* **95** (1991) 5981.

[9] Wynn C.H. and Robson B., *J. Theor. Biol.* **123** (1986) 221.

[10] Acquotti D., Poppe L., Dubrowski J., von der Lieth C.-W., Sonnino S. and Tettamanti G., *J. Am. Chem. Soc.* **112** (1990) 7772.

[11] The right hand side of equation (23) contains an additional term coming out from the translational entropies of α and β micelles which have different average aggregation numbers. It can be shown that the ratio between the leading and neglected term is proportional to $T_c/\gamma A^{(0)}$ which is of the order of 0.1 for reasonable values of the physical parameters.

[12] Brown R.E. and Hyland K.J., *Biochemistry* **31** (1992) 10602.

[13] Tettamanti G., Sonnino S., Ghidoni R., Masserini M. and Venerando B., in Physics of Amphiphiles: Micelles, Vesicles and Microemulsions, V. Degiorgio and M. Corti Eds. (North Holland, Amsterdam, 1985) pp. 607-636.

[14] Lofgren H. and Pascher I., *Chem. Phys. Lipids* **20** (1977) 273.

[15] Nores G. A., Dohi T., Taniguchi M. and Hakomori S. I., *J. Immunology* **139** (1987) 3171.

[16] Cantu' L., Corti M., Del Favero E., Digirolamo E., Sonnino S. and Tettamanti G., *Chem. Phys. Lipids*, to appear.

[17] Maggio B., Ariga T., Sturtevant J. M. and Yu R. K., *Biochemistry* **24** (1985) 1084.

[18] For amphiphiles, like gangliosides, with bulky head groups the surface area (and therefore the packing parameter) is practically unaffected by temperature-depending conformational variations of the hydrocarbon region.

[19] Cantu' L., Corti M., Sonnino S. and Tettamanti G., *Chem. Phys. Lipids* **41** (1986) 315.

[20] Gradshtein I. S. and Ryzhik I. M., Tables of Integrals, Series and Products (Academic Press, London, 1980).

[21] Taniguchi T., Kawasaki K., Andelman D. and Kawakatsu T., *J. Phys. II France* **4** (1994) 1333.